




Non-Reciprocal MEMS Periodic Structure

Jacopo Marconi * , Davide Enrico Quadrelli  and Francesco Braghin 

Department of Mechanical Engineering, Politecnico di Milano, Via La Masa 1, 20156 Milano, Italy; francesco.braghin@polimi.it (F.B.)

* Correspondence: jacopo.marconi@polimi.it

Abstract: In recent years, active periodic structures with in-time modulated parameters have drawn ever-increasing attention due to their peculiar (and sometimes exotic) wave propagation properties. Although many experimental works have shown the efficacy of time-modulation strategies, the benchmarks proposed until now have been mostly proof-of-concept demonstrators, with little attention to the feasibility of the solution for practical purposes. In this work, we propose a micro electro-mechanical system (MEMS) periodic structure with modulated electromechanical stiffness featuring non-reciprocal band-gaps that are frequency bands where elastic waves are allowed to travel only in one direction. To this aim, we derive a simplified analytical lumped-parameter model, which is then verified through numerical simulations of both the lumped-parameter system and the high-fidelity multiphysics finite element model including electrostatic effects. We envision that this system, which can easily be manufactured through standard MEMS production processes, may be used as a directional filter in MEMS devices such as insulators and circulators.

Keywords: periodic structures; MEMS; non-reciprocal; time modulation

1. Introduction

In mechanics, periodic structures are systems composed of the repetition of a unitary cell with a well-defined topology and physical properties [1]. In the last few decades, they have drawn an ever-increasing interest due to their ability to manipulate the propagation of waves in a number of different ways [2]. From a mechanical standpoint, vibration insulation and filtering are possibly their most interesting applications. Periodic structures indeed feature frequency bands, known as *band-gaps*, where wave propagation is hindered.

In recent years, a wealth of works dealing with periodic structures with (periodically) time-varying properties have shown that even more complex phenomena can be attained: selective wave filtering [3], topological pumping [4], and non-reciprocal wave transmission [5] are a few examples. The latter consists, loosely speaking, of the fact that wave propagation in a non-reciprocal medium is different depending on the propagation direction. In the context of periodic structures, this reveals in the presence of the so-called *directional band-gaps* and in a non-symmetric dispersion diagram [5–9]. In other words, depending on the propagation direction, one may find band-gaps that are not present if traveling in a different direction. In the case of 1D periodically modulated waveguides, directional band-gaps for right and left-propagating waves will appear in different frequency intervals, thus realizing a directional filter. Many benchmarks have already been proposed in the literature, as in [8], where an array of masses coupled through piloted magnets have been studied, and in [7], where an elastic beam with periodic shunted piezoelectric patches was experimentally tested. These solutions, however, are mainly proof-of-concept demonstrators.

In this work, we propose a micro electro-mechanical system (MEMS) periodic structure that can be used as a directional filter. In Radio Frequency (RF) applications, indeed, non-reciprocal components have long been used for filters, insulators, and circulators [10,11]. Given the high demand for these components in modern telecommunication systems,



Citation: Marconi, J.; Enrico Quadrelli, D.; Braghin, F. Non-Reciprocal MEMS Periodic Structure. *Actuators* **2023**, *12*, 161. <https://doi.org/10.3390/act12040161>

Academic Editor: Giorgio Olmi

Received: 16 February 2023

Revised: 27 March 2023

Accepted: 2 April 2023

Published: 4 April 2023



Copyright: © 2023 by the authors. Licensee MDPI, Basel, Switzerland. This article is an open access article distributed under the terms and conditions of the Creative Commons Attribution (CC BY) license (<https://creativecommons.org/licenses/by/4.0/>).

MEMS filters [12] and non-reciprocal filters [13,14] have also been proposed to reduce the footprint area of these devices and lower the production costs. To the best of the authors' knowledge, however, all these implementations rely upon different kinds of electric circuit resonators and typically operate in the range of MHz or even GHz. The solution we propose in this work, instead, uses a mechanical array of resonators, whose equivalent mechanical properties are modulated by means of the electrostatic forces at the interface of properly placed parallel plate electrodes. For this reason, the layout we propose can even be designed to work at frequencies in the range of a few tens of kHz.

The paper is organized as follows. In Section 2, a simplified electromechanic model for the unitary cell of the system is derived; in Section 3, with the aid of a continuum model, we find analytic expressions for the key parameters defining the non-symmetric dispersion diagram of the structure; in Section 4, we numerically verify our model by means of a high-fidelity multiphysics finite element model. Finally, conclusions are drawn in Section 5.

2. The Model

The system we propose is a 1-dimensional periodic waveguide, basically consisting of a spring-mass chain with elastic suspensions and where each mass hosts a fixed electrode in a dedicated cavity. Like the majority of inertial MEMS, the system features a 2D geometry, which is imposed by the etching process of the silicon wafer. In this context, springs are typically realized using folded beams [15]. The unitary cell of the periodic structure is in turn composed of $R = 3$ sub-cells, with three being the minimum number of sub-cells to obtain a wave-like traveling stiffness profile required to observe a non-reciprocal behavior [16]. The stiffness modulation, as already mentioned, is achieved by regulating the electrostatic forces acting between the fixed electrodes and the masses. The system is qualitatively represented in Figure 1.

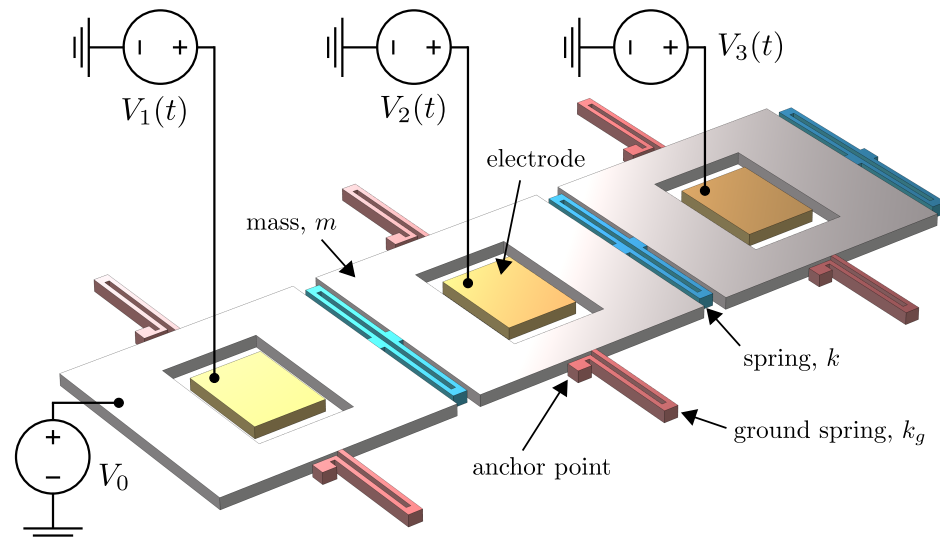


Figure 1. Unitary cell composed of three sub-cells. The masses (gray) are connected to each other through folded beams (blue) and to the ground (red). The electrodes (yellow) are fixed and placed in the hollowed masses. While the structure is set to a constant voltage V_0 , an alternate voltage $V_i(t)$ is imposed to each electrode i .

Let us now consider the sub-cell depicted in Figure 2, where the mass m is connected to the following/preceding mass and to the ground by springs of elastic constant k and k_g , respectively. For the i -th mass, the equation of motion writes

$$m\ddot{x}_i + (2k + k_g)x_i - kx_{i-1} - kx_{i+1} - f_{el} = 0, \quad (1)$$

where f_{el} is the net electrostatic force acting on the mass. Considering only the right side of the electrode, we can write its capacity as

$$C_R(x) = \frac{\epsilon A}{x + x_0}, \tag{2}$$

where ϵ is the vacuum permittivity constant, A the area, and x_0 the gap at rest. The electromechanical attractive force can then be obtained from the capacitor potential energy U as

$$f_{el,R} = \frac{\partial U}{\partial x} = \frac{1}{2} \frac{\partial C_R}{\partial x} \Delta V^2 = -\frac{1}{2} \frac{\epsilon A}{(x + x_0)^2} \Delta V^2, \tag{3}$$

with $\Delta V = \tilde{V}_i - V_0$, \tilde{V}_i is the time-varying voltage applied to the electrode, and V_0 the constant voltage applied to the structure. Using a Taylor expansion about $x = 0$ and neglecting $\mathcal{O}(x^4)$ terms, we can write

$$f_{el,R} \approx -\frac{\epsilon A}{2} \left(\frac{1}{x_0^2} - \frac{2}{x_0^3}x + \frac{3}{x_0^4}x^2 - \frac{4}{x_0^5}x^3 \right) \Delta V^2. \tag{4}$$

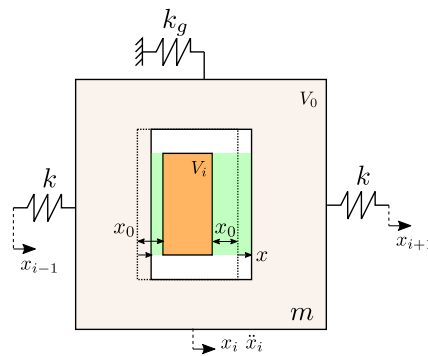


Figure 2. Sub-cell scheme considering a mass displaced by x . The area of interest for electrostatic forces is highlighted in light green.

In the same way, for the left side, we have

$$f_{el,L} = \frac{1}{2} \frac{\epsilon A}{(x - x_0)^2} \Delta V^2 \approx \frac{\epsilon A}{2} \left(\frac{1}{x_0^2} + \frac{2}{x_0^3}x + \frac{3}{x_0^4}x^2 + \frac{4}{x_0^5}x^3 \right) \Delta V^2, \tag{5}$$

so that, summing the two contributions, we have that the net electrostatic force is

$$f_{el} = f_{el,L} - f_{el,R} \approx \epsilon A \left(\frac{2}{x_0^3}x + \frac{4}{x_0^5}x^3 \right) \Delta V^2. \tag{6}$$

As it can be observed, this configuration is self-equilibrated (electrostatic forces are null for $x = 0$) and extends the linearity range of the parallel plate capacitor since the quadratic terms are canceled out. Additionally, it can be seen how f_{el} introduces a linear and cubic voltage-dependant stiffness into the system. Setting the electrode tension to

$$\tilde{V}_i(t) = V_a \cos\left(\omega_m t - \frac{2i}{R}\pi\right) = V_a \cos\theta_i, \tag{7}$$

where $i = \{1, \dots, R\}$ is the sub-cell ordinal, $R = 3$, and ω_m is the modulation frequency, we can develop the squared voltage difference as

$$\Delta V^2 = \left(\frac{V_a^2}{2} + V_0^2 \right) - 2V_a V_0 \cos\theta_i + \frac{V_a^2}{2} \cos(2\theta_i). \tag{8}$$

Plugging (8) into (6), we obtain

$$f_{el} = (k_{E0} - k_{E1} \cos \theta_i + k_{E2} \cos(2\theta_i)) \left(1 + \frac{2}{x_0^2} x^2 \right) x, \tag{9}$$

where

$$k_{E0} = \frac{2\varepsilon A}{x_0^3} \left(\frac{V_a^2}{2} + V_0^2 \right), \quad k_{E1} = \frac{4\varepsilon A}{x_0^3} V_a V_0, \quad k_{E2} = \frac{\varepsilon A}{x_0^3} V_a^2. \tag{10}$$

According to (9), the electrostatic stiffness features a constant term and two harmonics at ω_m and $2\omega_m$ (for both the linear and cubic terms). However, considering typical values $V_0 \sim 10$ V and $V_a \sim 1$ V, we have that

$$\frac{k_{E1}}{k_{E2}} = \frac{4V_0}{V_1} \sim 40, \tag{11}$$

and we can neglect the second harmonic.

Under the hypotheses of small displacements, we can also neglect the cubic stiffness, and, substituting the electrostatic forces in the equation of motion, we can finally write

$$m\ddot{x}_i + (2k + k_g - k_{E0} + k_{E1} \cos \theta_i)x_i - kx_{i-1} - kx_{i+1} = 0 \tag{12}$$

and recast the equations of motion for the i-th cell in matrix form as

$$\mathbf{M}\ddot{\mathbf{x}}_i + \mathbf{K}(t)\mathbf{x}_i - \mathbf{K}_L\mathbf{x}_{i-1} - \mathbf{K}_R\mathbf{x}_{i+1} = \mathbf{0}, \tag{13}$$

where \mathbf{x}_i is the displacement vector of the i-th cell, \mathbf{x}_{i-1} and \mathbf{x}_{i+1} are the neighboring cell displacement vectors, while $\mathbf{K}_{L/R}$ are the corresponding left/right stiffness matrices, so that Equation (13) writes:

$$\begin{aligned} & \begin{bmatrix} m & 0 & 0 \\ 0 & m & 0 \\ 0 & 0 & m \end{bmatrix} \begin{Bmatrix} \ddot{x}_1 \\ \ddot{x}_2 \\ \ddot{x}_3 \end{Bmatrix} - \begin{bmatrix} 0 & 0 & k \\ 0 & 0 & 0 \\ 0 & 0 & 0 \end{bmatrix} \begin{Bmatrix} x_{-2} \\ x_{-1} \\ x_0 \end{Bmatrix} - \begin{bmatrix} 0 & 0 & 0 \\ 0 & 0 & 0 \\ k & 0 & 0 \end{bmatrix} \begin{Bmatrix} x_4 \\ x_5 \\ x_6 \end{Bmatrix} + \\ & \begin{bmatrix} k^* + k_{E1} \cos \theta_1(t) & 0 & 0 \\ 0 & k^* + k_{E1} \cos \theta_2(t) & 0 \\ 0 & 0 & k^* + k_{E1} \cos \theta_3(t) \end{bmatrix} \begin{Bmatrix} x_1 \\ x_2 \\ x_3 \end{Bmatrix} = 0 \tag{14} \end{aligned}$$

where $k^* = 2k + k_g - k_{E0}$. Using this formalism, the asymmetric dispersion relation for the lumped-parameter spatiotemporal cell can be computed with the Bloch Based Procedure (BBP) illustrated in [6].

3. Parametric Analysis for Harmonic Modulation

In this section, we derive the modulation parameters that can be used to design a structure satisfying a user-tailored dispersion relation. This can be performed, in theory, by analyzing the quadratic eigenvalue problem (Q EVP) stemming from the application of the BBP to (13). However, even considering the simple case (described until now) of three masses and truncating the solution to the first harmonic, the resulting equations feature high-order polynomials with no closed-form solution. To circumvent this problem, we turn to the analysis of a rod with elastic suspensions, which is the continuum equivalent of a spring-mass chain system, and we seek a solution using the well-known Plane Wave Expansion Method (PWEM) [17].

3.1. Dispersion Relation for Rod on Elastic Foundations

Considering a rod with Young’s modulus E , density ρ , and cross-section area A , the governing equation writes

$$EA \frac{\partial^2 u}{\partial x^2} - \gamma u = \rho A \frac{\partial^2 u}{\partial t^2}, \tag{15}$$

where γ is the distributed ground stiffness and is modulated as

$$\gamma(x, t) = \gamma_0 + \gamma_m \cos(\omega_m t - \kappa_m x), \tag{16}$$

where γ_0 and γ_m are constant, and $\kappa_m = 2\pi/\lambda_m$ is the modulation wavenumber, with λ_m as the spatial periodicity of the spatiotemporal cell. To apply PWEM, both Floquet solution u and stiffness γ are expanded in a Fourier series as

$$u = \sum_{n=-\infty}^{+\infty} \hat{u}_n e^{i((\omega+n\omega_m)t - (\kappa+n\kappa_m)x)}, \quad \gamma = \sum_{p=-\infty}^{+\infty} \hat{\gamma}_p e^{ip(\omega_m t - \kappa_m x)}, \tag{17}$$

which are first truncated to order N and then plugged into (15). Exploiting the orthogonality property of the Fourier series, one can rid of the double summation generated by the γu term, and finally, write a set of equations

$$EA(\kappa + q\kappa_m)^2 \hat{u}_q + \sum_{n=-N}^N \hat{\gamma}_{q-n} \hat{u}_n = \rho A(\omega + q\omega_m)^2 \hat{u}_q, \tag{18}$$

where $q \in \mathbb{Z}$ is an additional index. Writing a number $2N + 1$ of the above equation for $q \in \{-N, \dots, N\}$, a square system in the coefficients \hat{u}_q is obtained and, in matrix form, writes as

$$\left(\mathbf{L}_0(\kappa) + \omega \mathbf{L}_1 + \omega^2 \mathbf{L}_2 \right) \hat{\mathbf{u}} = \mathbf{L}(\kappa, \omega) \hat{\mathbf{u}} = 0, \tag{19}$$

which is a QEVP that can be solved by imposing κ , and where $\hat{\mathbf{u}} = [\hat{u}_N, \dots, \hat{u}_{-N}]^T$. For each κ , then $2(2N + 1)$ eigenfrequencies are obtained and the dispersion diagram can be drawn.

3.2. Dispersion Analysis

To derive simplified formulas for the dispersion key characteristics, namely, directional bandgap positions and amplitude, with respect to the modulation parameters, we loosely retrace the steps presented in [5] for a simple rod with no elastic suspensions.

First, setting $N = 1$, we retain only the first harmonic in the solution. We also notice that for the harmonic modulation in (16), the Fourier coefficients are $\hat{\gamma}_0 = \gamma_0$, $\hat{\gamma}_{\pm 1} = \gamma_m/2$, and $\hat{\gamma}_p = 0$ for $|p| \geq 2$. Let us define

$$\omega_\gamma = \sqrt{\frac{\hat{\gamma}_0}{\rho A}}, \quad \omega_a = \sqrt{\frac{\hat{\gamma}_1}{\rho A}}, \tag{20}$$

and the following dimensionless quantities

$$\Omega_\star = \frac{\omega_\star \lambda_m}{2\pi c_0}, \quad \mu = \kappa \lambda_m, \tag{21}$$

where \star denotes a generic subscript and where $c_0 = \sqrt{E/\rho}$. Using the expressions above, we can write a 3×3 dimensionless QEVP as

$$\mathbf{L}(\mu, \Omega) = 0, \tag{22}$$

where the components of \mathbf{L} are

$$L_{11} = \left(\frac{\mu}{2\pi} + 1\right)^2 - (\Omega + \Omega_m)^2 + \Omega_\gamma^2, \quad (23)$$

$$L_{22} = \left(\frac{\mu}{2\pi}\right)^2 - \Omega^2 + \Omega_\gamma^2, \quad (24)$$

$$L_{33} = \left(\frac{\mu}{2\pi} - 1\right)^2 - (\Omega - \Omega_m)^2 + \Omega_\gamma^2, \quad (25)$$

$$L_{12} = L_{21} = L_{23} = L_{32} = \Omega_a^2. \quad (26)$$

As conducted in [5], we can focus on the forward and backward directional band-gaps *separately* by considering the partitions of $\mathbf{L}(\mu, \Omega)$ pertaining to $\{\hat{u}_0, \hat{u}_{-1}\}$ and $\{\hat{u}_0, \hat{u}_{+1}\}$, respectively. This way, the characteristic equation for the backward directional band-gap writes

$$L_{11}L_{22} - L_{12}L_{21} = 0, \quad (27)$$

that is,

$$\left(\left(\frac{\mu}{2\pi} + 1\right)^2 - (\Omega + \Omega_m)^2 + \Omega_\gamma^2\right) \left(\left(\frac{\mu}{2\pi}\right)^2 - \Omega^2 + \Omega_\gamma^2\right) = -\Omega_a^2. \quad (28)$$

The above equation is quartic; however, in the limit $\Omega_a \rightarrow 0$ (no modulation), it turns into two separate quadratic algebraic equations, whose solutions are

$$\Omega_{1,2} = \pm \sqrt{\Omega_\gamma^2 + \left(\frac{\mu}{2\pi}\right)^2}, \quad (29)$$

$$\Omega_{3,4} = -\Omega_m \pm \sqrt{\Omega_\gamma^2 + \left(\frac{\mu}{2\pi} + 1\right)^2}. \quad (30)$$

Similarly, from $L_{22}L_{33} = 0$, we obtain

$$\Omega_{5,6} = +\Omega_m \pm \sqrt{\Omega_\gamma^2 + \left(\frac{\mu}{2\pi} - 1\right)^2}. \quad (31)$$

We can now obtain the wave number where the branches intersect by solving $\Omega_1 = \Omega_3$ and $\Omega_1 = \Omega_5$ for μ :

$$\mu_{F,B} = \pm\pi(1 \pm \Omega_m\sigma), \quad (32)$$

where

$$\sigma = \sqrt{1 + \frac{4\Omega_\gamma^2}{1 - \Omega_m^2}}. \quad (33)$$

The corresponding frequencies, finally, write

$$\Omega_{F,B} = \Omega_1(\mu_{F/B}) = \sqrt{\Omega_\gamma^2 + \frac{(1 \pm \Omega_m\sigma)^2}{4}}, \quad (34)$$

so that the positions of the directional band-gaps openings are defined by the two sets $\{\mu_B, \Omega_B\}$ and $\{\mu_F, \Omega_F\}$. The frequency separation between these two points can be computed as the difference

$$\Delta\Omega_{FB} = \Omega_F - \Omega_B = \frac{\Omega_m\sigma}{\sqrt{\Omega_\gamma^2 + (1 + \Omega_m\sigma)^2/4} + \sqrt{\Omega_\gamma^2 + (1 - \Omega_m\sigma)^2/4}}, \quad (35)$$

which, considering $\Omega_m \ll 1$, can be approximated as

$$\Delta\Omega_{FB} \approx \frac{\Omega_m \sigma}{\sqrt{1 + 4\Omega_\gamma^2}} \approx \Omega_m. \tag{36}$$

The analytic dispersion branches and the parameters derived above are shown in Figure 3a and compared to the numerical results obtained by exactly solving (22).

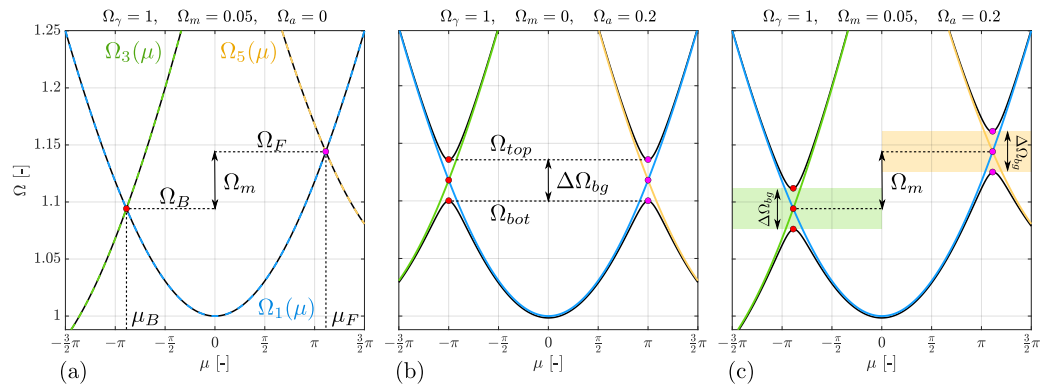


Figure 3. Dispersion relations for a rod on elastic suspensions with space–time modulation. Numerical results (black lines) are compared to the analytic results (colored lines), and key properties are shown on the dispersion diagrams for completeness. (a) Case with no amplitude modulation ($\gamma_m = 0$); (b) with constant properties in time ($\omega_m = 0$); (c) with both modulations active.

Another important parameter to consider is the band-gap amplitude. Previous works have shown that this usually has only a second-order dependence on the modulation speed; differently from [5], we thus conduct this analysis setting $\Omega_m = 0$. In this case, the dispersion is symmetric, so we can also set $\mu = \pi$. Under these hypotheses, one can again solve the characteristic equation $L_{11}L_{22} - L_{12}^2 = 0$ for Ω , obtaining

$$\Omega_{top} = \sqrt{\frac{1}{4} + \Omega_\gamma^2 + \Omega_a^2}, \quad \Omega_{bot} = \sqrt{\frac{1}{4} + \Omega_\gamma^2 - \Omega_a^2}, \tag{37}$$

for the top and bottom frequencies of the band-gap, so that the amplitude writes

$$\Delta\Omega_{bg} = \Omega_{top} - \Omega_{bot} = \frac{2\Omega_a^2}{\sqrt{\frac{1}{4} + \Omega_\gamma^2 + \Omega_a^2} + \sqrt{\frac{1}{4} + \Omega_\gamma^2 - \Omega_a^2}} \approx \frac{\Omega_a^2}{\sqrt{\frac{1}{4} + \Omega_\gamma^2}}, \tag{38}$$

where the last approximation is taken, considering that $\Omega_\gamma^2 \gg \Omega_a^2$. The band-gap amplitude is reported in the diagrams of Figure 3b for $\Omega_m = 0$ and in Figure 3c for $\Omega_m = 0.05$, showing in both cases accurate predictions in spite of the approximations. Finally, it is straightforward to observe that we have complete separation of the directional band-gaps (i.e., with no overlap) for a modulation speed $\Omega_m \geq \Omega_{m,lim} = \Delta\Omega_{bg}$.

3.3. From Rod to Spring-Mass Chain

As mentioned at the beginning of this section, a spring-mass chain can be seen as the discrete approximation of a rod. We can use the following relationships to switch from the rod parameters to spring-mass chain ones:

$$m = \rho Aa, \quad k = \frac{EA}{a}, \quad k_g = \gamma a, \quad c_0 = a\sqrt{\frac{k}{m}} \tag{39}$$

with $a = \lambda_m/R$ being the distance between two adjacent masses and R the number of masses per spatial period (which was assumed equal to 3 in the previous section).

In Figure 4, we show the comparison of the dispersion relations for a space-time modulated rod (obtained with PWEM) and its spring-mass chain counterpart (obtained with the BBP). These results were obtained by fixing the rod properties to $EA = \rho A = 1$, $\gamma_0 = 10$, $\gamma_m = 5$, $\lambda_m = 1$, $\Omega_m = \Omega_{m,lim}$, and letting R vary. As it can be observed, the spring-mass chain’s diagram converges to the rod’s one, increasing the number of masses (i.e., sub-cells). In the case of the minimum number of sub-cells $R = 3$, the diagrams slightly drift apart; however, band-gap positions are very close to the ones predicted with the rod model, and their widths are almost the same. Upon these observations, we can finally conclude that the analytic formulae derived in this section for a rod on elastic suspensions can be usefully exploited to guide the design of a spring-mass chain system.

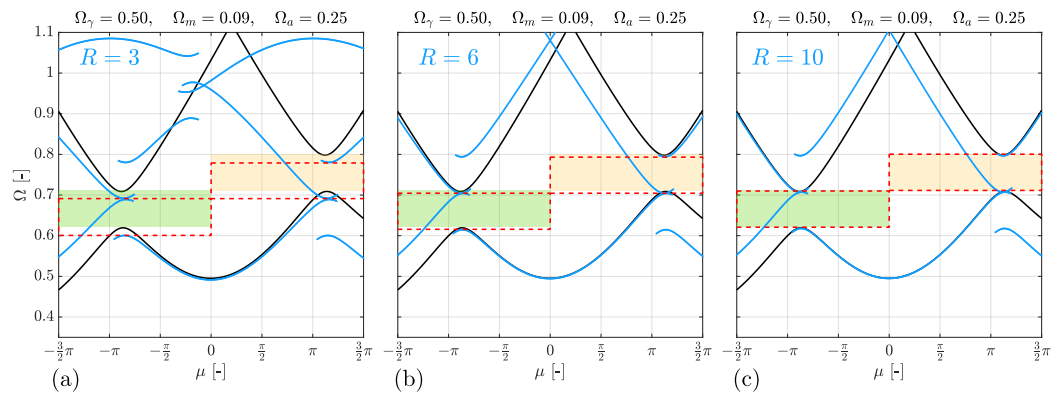


Figure 4. Comparison between the dispersion diagrams of a rod (black line) and of its spring-mass chain discretization (blue line), using $R = 3, 6, 10$ masses (a–c). Directional band-gaps predicted with the rod model are highlighted in green and yellow, while the band-gaps of the spring-mass chain system are enclosed in dashed red boxes.

4. Numerical Study of the MEMS Device

In this section, we numerically study an example of a finite-size system, with typical MEMS dimensions, composed of the unitary cells introduced in Section 2 and qualitatively depicted in Figure 1. As anticipated, we use $R = 3$ masses per cell, accepting a small drift from the continuous rod case with the aim to reduce the size and complexity of the system. With reference to the scheme in Figure 5, we can define the geometrical dimension of our system by setting the values of the lumped parameters appearing in (12) and by using the following equations

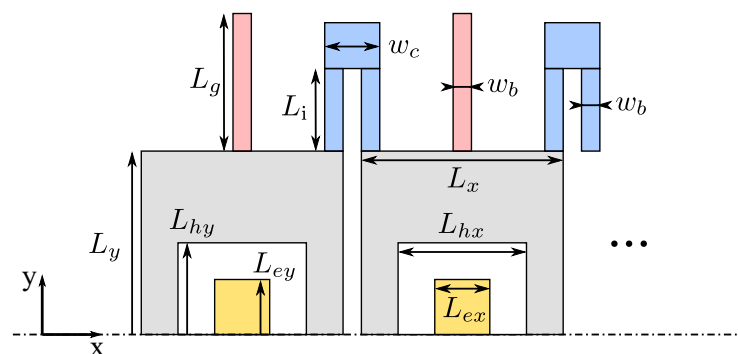


Figure 5. Scheme of the geometry of the COMSOL model (only 2 sub-cells are shown). The dashed-dotted line denotes a symmetry axis.

$$m = \rho t(L_x L_y - L_{hx} L_{hy}), \tag{40}$$

$$k_g = 2 \frac{E w_b^3 t}{L_g^3}, \quad k = \frac{2}{N_F} \frac{E w_b^3 t}{L_i^3}, \quad (41)$$

where factor 2 in the stiffness definitions is to take into account the fact that the beams come in pairs as parallel springs, and where $N_F = 2$ is the number of folds. In the same way, setting the desired electrical stiffness in (10), we can define the electrode dimensions from

$$A = L_{ey}t, \quad x_0 = (L_{hx} - L_{ex})/2. \quad (42)$$

Notice that the stiffness modulation parameters k_{E0} and k_{E1} both depend on the voltages V_0 and V_a ; however, since the former depends on $V_0^2 + V_a^2$ and the latter on $V_0 V_a$, if $V_0 \gg V_a$, we can tune k_{E0} by setting V_0 and k_{E1} changing V_a . All the geometric, mechanical, and electric parameters are collected in Tables 1–3.

Table 1. Geometric parameters (in μm), as shown in Figure 5.

$L_g = 150$	$L_i = 150$	$L_x = 100$	$L_y = 200$
$L_{ex} = 5$	$L_{ey} = 100$	$L_{hx} = 7$	$L_{hy} = 102$
$x_0 = 1$	$w_b = 2$	$w_c = 8$	

Table 2. Mechanical and electrical parameters.

$E = 148$ [GPa]	silicon elastic modulus
$\rho = 2330$ [kg/m^3]	silicon density
$t = 10$ [μm]	silicon wafer thickness
$\lambda_m = 312$ [μm]	cell spatial period
$\varepsilon = 8.854 \times 10^{-12}$ [F/m]	vacuum permittivity
$V_a = 2$ [V]	AC voltage amplitude
$V_0 = 14$ [V]	DC voltage amplitude
$\omega_m = 12,500$ [rad/s]	voltage modulation frequency

Table 3. Spring-mass chain lumped parameters.

$k = 3.51$ [N/m]	stiffness between masses
$k_g = 7.02$ [N/m]	ground stiffness
$k_{E0} = 3.51$ [N/m]	constant electrostatic stiffness
$k_{E1} = 0.99$ [N/m]	time-modulated electrostatic stiffness
$m = 44.81$ [ng]	mass value

For the numerical verification, we simulate the system with an electromechanical model in COMSOL Multiphysics to take into account in full the effect of the electrostatic forces exerted by the modulated electrodes. The system is composed of $N_c = 40$ cells and is forced in the middle of the chain with a tone burst. The tone burst's central frequency is in between the two directional band-gaps. This way, both right and left-propagating waves can be analyzed with a single run. Moreover, the amplitude of the forcing is chosen in order not to trigger nonlinear effects in the electrostatic domains (the maximum mass displacement is less than 2% of the gap amplitude x_0 – with reference to (6), the ratio between the linear and cubic terms is equal to $(x_0/x)^2/2$, so that the former is three orders of magnitude higher than the latter).

The results are shown in Figure 6. As it can be observed, the numerical dispersion closely matches the spring-mass chain model prediction, with only a small drift due to the flexibility of the masses and of the beam connections, which are not accounted for in the analytic formulae for the springs. The dimensionless parameters introduced in Section 3 also match: the shift of the band-gaps is equal to $\Omega_m = 0.07$ (1990 Hz), the band-gap amplitude is approximately $\Delta\Omega_{bg} = 0.05$ (1300 Hz), and the cutoff frequency of the system is given by $\Omega_\gamma = 0.48$ (14.1 kHz).

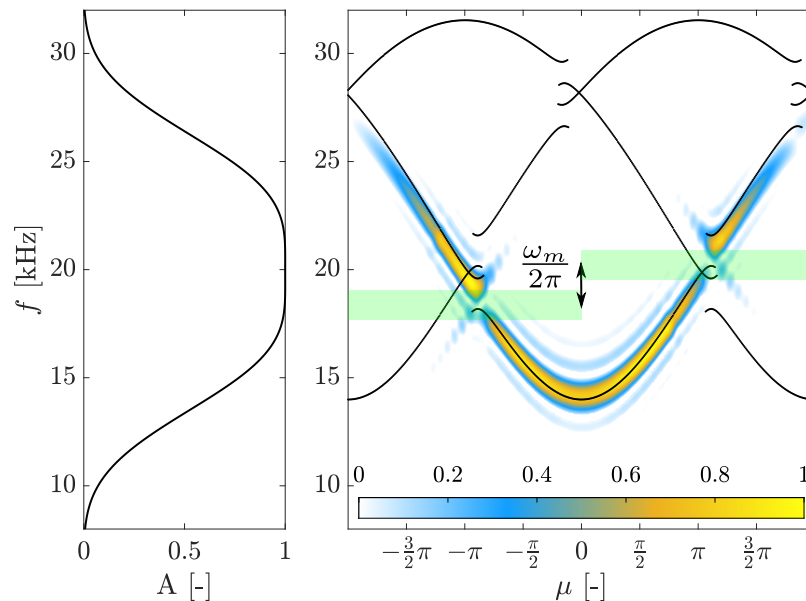


Figure 6. Numerical dispersion, obtained with the COMSOL Multiphysics model, vs. analytical prediction (black line), obtained with the spring-mass chain model and the BBP (**right**) and spectrum of the input tone burst (**left**).

5. Conclusions

In this work, we analyzed a one-dimensional periodic waveguide with periodically time-varying properties. The system consists of a spring-mass chain system resting on elastic foundations, whose stiffness is modulated by means of the electrostatic forces exerted by the parallel plate electrodes collocated inside the masses. We first derived a simplified model, valid for small displacement around the equilibrium, and we fully characterized its dispersion relation through the study of its continuum equivalent (rod system). Finally, our model has been validated against the numerical results of a high-fidelity model in COMSOL Multiphysics. The proposed system can be readily produced using standard MEMS technologies and, as demonstrated by the dimensionless analysis of the dispersion, can be easily tailored to work in different frequency ranges, going (considering typical MEMS dimensions) from a few kHz onward, just by properly selecting the spring-mass chain parameters. For this reason, the presented layout can be both interesting to be used for new low-frequency applications and/or to replace already existing components in high-frequency ones.

Author Contributions: Conceptualization, J.M.; Software, D.E.Q.; Formal analysis, J.M. and D.E.Q.; Writing—original draft, J.M.; Writing—review & editing, D.E.Q.; Supervision, F.B.; Funding acquisition, F.B. All authors have read and agreed to the published version of the manuscript.

Funding: This research received no external funding.

Data Availability Statement: Data can be made available upon reasonable request to the authors.

Conflicts of Interest: The authors declare no conflict of interest.

References

1. Hussein, M.I.; Leamy, M.J.; Ruzzene, M. Dynamics of phononic materials and structures: Historical origins, recent progress, and future outlook. *Appl. Mech. Rev.* **2014**, *66*, 040802. [[CrossRef](#)]
2. Kadic, M.; Milton, G.W.; van Hecke, M.; Wegener, M. 3D metamaterials. *Nat. Rev. Phys.* **2019**, *1*, 198–210. [[CrossRef](#)]
3. Trainiti, G.; Xia, Y.; Marconi, J.; Cazzulani, G.; Erturk, A.; Ruzzene, M. Time-periodic stiffness modulation in elastic metamaterials for selective wave filtering: Theory and experiment. *Phys. Rev. Lett.* **2019**, *122*, 124301. [[CrossRef](#)] [[PubMed](#)]
4. Xia, Y.; Riva, E.; Rosa, M.I.; Cazzulani, G.; Erturk, A.; Braghin, F.; Ruzzene, M. Experimental observation of temporal pumping in electromechanical waveguides. *Phys. Rev. Lett.* **2021**, *126*, 095501. [[CrossRef](#)] [[PubMed](#)]

5. Trainiti, G.; Ruzzene, M. Non-reciprocal elastic wave propagation in spatiotemporal periodic structures. *New J. Phys.* **2016**, *18*, 083047. [[CrossRef](#)]
6. Vila, J.; Pal, R.K.; Ruzzene, M.; Trainiti, G. A bloch-based procedure for dispersion analysis of lattices with periodic time-varying properties. *J. Sound Vib.* **2017**, *406*, 363–377. [[CrossRef](#)]
7. Marconi, J.; Riva, E.; Di Ronco, M.; Cazzulani, G.; Braghin, F.; Ruzzene, M. Experimental observation of nonreciprocal band gaps in a space-time-modulated beam using a shunted piezoelectric array. *Phys. Rev. Appl.* **2020**, *13*, 031001. [[CrossRef](#)]
8. Chen, Y.; Li, X.; Nassar, H.; Norris, A.N.; Daraio, C.; Huang, G. Nonreciprocal wave propagation in a continuum-based metamaterial with space-time modulated resonators. *Phys. Rev. Appl.* **2019**, *11*, 064052. [[CrossRef](#)]
9. Nassar, H.; Yousefzadeh, B.; Fleury, R.; Ruzzene, M.; Alù, A.; Daraio, C.; Norris, A.N.; Huang, G.; Haberman, M.R. Nonreciprocity in acoustic and elastic materials. *Nat. Rev. Mater.* **2020**, *5*, 667–685. [[CrossRef](#)]
10. Yu, Y.; Michetti, G.; Pirro, M.; Kord, A.; Sounas, D.L.; Xiao, Z.; Cassella, C.; Alu, A.; Rinaldi, M. Radio Frequency Magnet-Free Circulators Based on Spatiotemporal Modulation of Surface Acoustic Wave Filters. *IEEE Trans. Microw. Theory Technol.* **2019**, *67*, 4773–4782. [[CrossRef](#)]
11. Ashley, A.; Psychogiou, D. RF Co-Designed Bandpass Filters/Isolators Using Nonreciprocal Resonant Stages and Microwave Resonators. *IEEE Trans. Microw. Theory Technol.* **2021**, *69*, 2178–2190. [[CrossRef](#)]
12. Weinstein, D.; Bhawe, S.A.; Tada, M.; Mitarai, S.; Morita, S.; Ikeda, K. Mechanical coupling of 2D resonator arrays for MEMS filter applications. In Proceedings of the 2007 IEEE International Frequency Control Symposium Joint with the 21st European Frequency and Time Forum, Geneva, Switzerland, 29 May–1 June 2007; IEEE: Piscataway, NJ, USA, 2007; pp. 1362–1365.
13. Pirro, M.; Cassella, C.; Michetti, G.; Chen, G.; Kulik, P.; Yu, Y.; Rinaldi, M. Novel topology for a non-reciprocal MEMS filter. In Proceedings of the 2018 IEEE International Ultrasonics Symposium (IUS), Kobe, Japan, 22–25 October 2018; IEEE: Piscataway, NJ, USA, 2018; pp. 1–3.
14. Yu, Y.; Michetti, G.; Kord, A.; Sounas, D.; Pop, F.V.; Kulik, P.; Pirro, M.; Qian, Z.; Alu, A.; Rinaldi, M. Magnetic-free radio frequency circulator based on spatiotemporal commutation of MEMS resonators. In Proceedings of the 2018 IEEE Micro Electro Mechanical Systems (MEMS), Belfast, UK, 21–25 January 2018; IEEE: Piscataway, NJ, USA, 2018, pp. 154–157.
15. Acar, C.; Shkel, A. *MEMS Vibratory Gyroscopes: Structural Approaches to Improve Robustness*; Springer: Berlin/Heidelberg, Germany, 2008.
16. Marconi, J.; Cazzulani, G.; Riva, E.; Braghin, F. Observations on the behavior of discretely modulated spatiotemporal periodic structures. In Proceedings of the Active and Passive Smart Structures and Integrated Systems XII, Denver, CO, USA, 5–8 March 2018; Erturk, A., Ed.; International Society for Optics and Photonics, SPIE: Cergy-Pontoise, France, 2018; Volume 10595, pp. 630–636. [[CrossRef](#)]
17. Riva, E.; Marconi, J.; Cazzulani, G.; Braghin, F. Generalized plane wave expansion method for non-reciprocal discretely modulated waveguides. *J. Sound Vib.* **2019**, *449*, 172–181. [[CrossRef](#)]

Disclaimer/Publisher’s Note: The statements, opinions and data contained in all publications are solely those of the individual author(s) and contributor(s) and not of MDPI and/or the editor(s). MDPI and/or the editor(s) disclaim responsibility for any injury to people or property resulting from any ideas, methods, instructions or products referred to in the content.